Received: 18 November 2020 | Revised: 5 March 2021 | Accepted: 17 March 2021

DOI: 10.1111/cas.14900

ORIGINAL ARTICLE

Cancer Science WILEY

MZT2A promotes NSCLC viability and invasion by increasing Akt phosphorylation via the MOZART2 domain

Huanxi Wang[1] | Xizi Jiang[1] | Yu Cheng[1,2] | Hongjiu Ren[1] | Yujiao Hu[1] | Yao Zhang[1] | Hongbo Su[1] | Zifang Zou[3] | Qiongzi Wang[1] | Zongang Liu[4] | Jiameng Zhang[1] | Xueshan Qiu[1,5]

[1]Department of Pathology, China Medical University, Shenyang, China

[2]Departemt of Pathology, Cancer Research Laboratory, Chengde Medical College, Chengde, China

[3]Department of Thoracic Surgery, The First Affiliated Hospital of China Medical University, Shenyang, China

[4]Department of Thoracic Surgery, Shengjing Hospital of China Medical University, Shenyang, China

[5]Department of Pathology, The First Affiliated Hospital of China Medical University, Shenyang, China

Correspondence
Xueshan Qiu, Department of Pathology, China Medical University, 77 Puhe Road, North Shenyang New Area, Shenyang, Liaoning 110122, China.
Email: xsqiu@cmu.edu.cn

Abstract

Mitotic spindle organizing protein 2A (MZT2A) is localized at the centrosome and regulates microtubule nucleation activity in cells. This study assessed the role of MZT2A in non–small-cell lung cancer (NSCLC). Differential MZT2A expression was bioinformatically assessed using TCGA database, the GEPIA database, and Kaplan-Meier survival data to determine the association between MZT2A expression and NSCLC prognosis. Furthermore, NSCLC tissue specimens were evaluated by immunohistochemistry. MZT2A was overexpressed or knocked down in NSCLC cells using cDNA and siRNA, respectively. The cells were subjected to various assays and treated with the selective Akt inhibitor LY294002 or co-transfected with galectin-3-binding protein (LGALS3BP) siRNA. MZT2A mRNA and protein levels were upregulated in NSCLC lesions and MTZ2A expression was associated with poor NSCLC prognosis. MZT2A protein was also highly expressed in NSCLC cells compared with the expression in normal bronchial cells. MZT2A expression promoted NSCLC cell viability and invasion, whereas MTZ2A siRNA had the opposite effect on NSCLC cells in vitro. At the protein level, MZT2A induced Akt phosphorylation, promoting NSCLC proliferation and invasion (but the selective Akt inhibitor blocked these effects) through upregulation of LGALS3BP via the MTZ2A MOZART2 domain, whereas LGALS3BP siRNA suppressed MTZ2A activity in NSCLC cells. The limited in vivo experiments confirmed the in vitro data. In conclusion, MZT2A exhibits oncogenic activity by activating LGALS3BP and Akt in NSCLC. Future studies will assess MTZ2A as a biomarker to predict NSCLC prognosis or as a target in the control of NSCLC progression.

KEYWORDS

Akt, LGALS3BP, MZT2A, NSCLC, prognosis

Abbreviations: GEPIA, Gene Expression Profiling Interactive Analysis; LGALS3BP, galectin 3 binding protein; LUAD, lung adenocarcinoma; LUSC, lung squamous cell carcinoma; MEM, modified Eagle's medium; MOZART2, mitotic spindle organizing protein associated with a ring of tubulin; MZT2A, mitotic spindle organizing protein 2A; NSCLC, non–small-cell lung cancer; TCGA, The Cancer Genome Atlas.

1 | INTRODUCTION

Lung cancer is the most commonly occurring cancer and the leading cause of cancer death globally, accounting for 11.6% of the 18.1 million new cases and 18.4% of the 9.6 million cancer-related deaths in 2018.[1] Histologically, up to 85% of all lung cancer cases are NSCLCs and the rest are small-cell lung cancers.[2-4] Most NSCLCs are diagnosed at advanced stages of the disease, making curable surgery impossible. Routine chemoradiation therapy is frequently ineffective for controlling NSCLCs, therefore the 5-y survival rate of NSCLC patients is only 10%-20% in most parts of the world.[5,6] In this regard, it is necessary for researchers to better understand the molecular mechanisms of NSCLC tumorigenesis. This will enable the development and identification of novel strategies or biomarkers for the prevention and treatment of this deadly disease and facilitate early diagnosis, as well as prediction of the treatment responses and prognosis of patients with lung cancer.[7,8]

Microtubules are dynamic and hollow tubular structures that form the cell cytoskeleton.[9-11] They consist at the molecular level of tubulin and microtubule accessory proteins and regulate biological processes such as cell mobility and gene expression in cells.[9-11] Microtubules are nucleated and organized by microtubule organizing centers, specifically the centrosome. Many proteins bind to microtubules, such as the motor proteins kinesin and dynein as well as microtubule-severing proteins, which regulate microtubule dynamics. The aberrant expression and/or activity of these proteins is associated with the development of breast,[12] lung,[13-15] liver,[16] gastric,[17,18] and thyroid cancers.[19] Targeting microtubulin proteins and their activity has been shown to be effective for the treatment of various human cancers,[20,21] although drug resistance remains an unresolved issue. The mitotic spindle organizing protein 2A (MZT2A; also known as GCP8a or FAM128A) mediates cell septation signaling during cell growth through a balance of microtubule polymerization and depolymerization at the centrosome.[22-24] MZT2A was initially identified in 2010 by Hutchins et al, who named the protein MOZART2.[22] Teixido-Travesa et al also identified MZT2A in 2010 as a protein in the γ-tubulin ring complex (γ-TuRC) with a size of up to 20 kDa.[24] Since then, it has become evident that a lack of MZT2A expression in cells can impair microtubule nucleation activity and slow the rate of cell proliferation.[22,24] Therefore, further exploration of MZT2A expression and activity in NSCLCs can help clinicians to effectively control NSCLC development and progression as a novel strategy for the development of biomarker and targeting therapies.

In this study, we first screened several online databases and performed bioinformatic analyses of differential MZT2A expression in these databases. We then assessed MZT2A expression in NSCLC tissue to determine any association with the prognosis of patients and also investigated the role of MZT2A in lung cancer cells in vitro.

2 | MATERIALS AND METHODS

2.1 | Databases and data analysis

In this study, we searched TCGA and GEPIA databases and analyzed Kaplan-Meier survival data. We then assessed differential MZT2A expression to determine any association with the prognosis for lung cancer. We first retrieved lung cancer data on MZT2A expression from TCGA database, which consisted of processed level 3 RNA-seq data and the corresponding clinical information for patients, and assessed differential MZT2A expression in NSCLCs vs. normal tissues. Next, we retrieved data from the GEPIA database and further analyzed differential MZT2A expression in LUAD and LUSC vs. normal tissues. We also performed Kaplan-Meier survival analysis to determine the association between MZT2A expression and NSCLC prognosis.

2.2 | Patients and specimens

We retrospectively analyzed tissue specimens collected from 224 patients with NSCLC who utilized in-patient services at the Pathology Department of the First Affiliated Hospital of China Medical University from 2013 to 2018. All patients underwent curative surgical resection without prior chemotherapy or radiation therapy and their NSCLC was diagnosed and classified according to TNM classification, 8th edition.[25] Paraffin blocks of paired tumor and normal tissues were retrieved, histologically re-confirmed, and used for this study. We also conducted follow-up and survival analysis on 45 patients included in this study from 2013 to 2016. This study was approved by the Medical Research Ethics Committee of China Medical University and informed consent was obtained from all patients.

2.3 | Immunohistochemistry

Buffered formalin-fixed and embedded paraffin blocks were retrieved from the Pathology Department and cut into 3-μm-thick consecutive sections. For immunohistochemistry, the tissue sections were first deparaffinized in xylene, rehydrated in a series of ethanol solutions, and blocked with normal goat non-immune serum (SP Kit-A3/B3, MaiXin). The sections were then incubated with an anti-MZT2A antibody at a dilution of 1:200 (Thermo) or an anti-galectin-3-binding protein (LGALS3BP) antibody at a dilution of 1:300 (Cat. 10281-1-AP; Proteintech) at 4°C overnight. The next day, the sections were washed in ice-cold PBS 3 times and further incubated with reagents A and B (KIT9921; MaiXin) according to the manufacturer's instructions. After the color reaction, the immunostained tissue sections were mounted with neutral resin. Afterward, the staining intensity and percentage were reviewed and scored semi-quantitatively by 2 investigators blinded to the clinical data. The staining intensity was rated as 0, (no staining of tumor cells), 1 (weak staining), 2 (moderate staining), or 3 (strong staining), while the percentage of staining was rated as 1 (0%-25% of tumor cells stained), 2 (26%-50%), 3 (51%-75%), or 4 (>76%). The 2 scores were then multiplied to obtain the staining index (between 0 and 12). A staining index >3 indicated high MZT2A expression, whereas a number ≤3 indicated low MZT2A expression. A staining index >5

indicated high LGALS3BP expression, whereas a number ≤5 indicated low LGALS3BP expression.

2.4 | Cell lines and culture

Human NSCLC-A549, NCI-H1299, NCI-H460, NCI-H226, NCI-H292, SK-MES-1, and NCI-H661 cell lines were obtained from the Cell Bank of the Chinese Academy of Sciences and maintained (except SK-MES-1) in Roswell Park Memorial Institute medium-1640 (RPMI-1640; Gibco) supplemented with 10% FBS (Clark Biosciences) in a humidified incubator at 5% CO_2 in air and 37°C. The normal human bronchial epithelial (HBE) cell line was obtained from the Cell Bank of the Chinese Academy of Sciences and cultured in DMEM with high glucose. SK-MES-1 cells were cultured in Eagle's MEM supplemented with 10% FBS under the same culture conditions.

2.5 | Plasmid construction and cell transfection

Plasmids carrying MZT2A cDNA and vector only were obtained from GenePharma, while MZT2A-specific small-interfering RNA (siRNA) and negative control siRNA were obtained from Riobobio. The LGALS3BP siRNA and negative control siRNA were obtained from GenePharma. We also constructed 2 MZT2A mutants with changes in the MOZART2 domain. The MOZART2 domain was knocked out in the first mutant (MZT2A-ΔMOZART2) while retaining the antibody recognition sequence. In the second mutant (MZT2A-MOZART2), all sequences were knocked out, with the exception of the MOZART2 domain and the antibody recognition sequences. After DNA-sequencing confirmation, the 2 plasmids were transfected into NSCLC cells. For cell transfection, cells were grown and transiently transfected with the above vectors or siRNAs using Lipofectamine 3000 reagent (Invitrogen, Carlsbad, CA, USA) for 48 h according to the manufacturer's protocol. After that, G418 (400 μg/mL) was added to the culture medium to establish stable MZT2A expression or mutant cell sublines. To suppress Akt signaling activity, after gene transfection for 36 h, cell lines were treated with 10 μmol/L LY294002 (MedChemExpress) dissolved in dimethyl sulfoxide (DMSO) for 12 h. DMSO treatment was used as the negative control. siRNA sequences targeting MZT2A or LGALS3BP and the plasmids carrying MZT2A cDNA are shown in Tables S1 and S2, respectively.

2.6 | Quantitative reverse transcriptase-polymerase chain reaction (RT-qPCR)

Total cellular RNA was isolated from the transient transfected cells using the TRIzol reagent (TransGen Biotech), quantified using a spectrophotometer (IMPLEN), and reverse transcribed into cDNA using the PrimeScript RT Master Mix kit (TaKaRa) according the manufacturer's instructions. cDNA samples were subjected to quantitative PCR (qPCR) amplification of the MZT2A, AKT, cyclinD1, CDK4, CDK6, RhoA, Vimentin and GAPDH mRNAs using specifically designed primers (Table S3) and the TB Green Premix EX *Taq* II Kit (TaKaRa). Relative mRNA levels were determined using the comparative method ($\Delta\Delta C_T$) followed by normalization to the GAPDH level (an internal control).

2.7 | Immunocytochemistry

A549, NCI-H1299, NCI-H460, and NCI-H292 cells were grown on coverslips and then collected and fixed in 4% paraformaldehyde for 20 min. Afterward, the cells were treated with 0.25% Triton-X100 at room temperature for 15 min, blocked in 5% BSA in PBS at 37°C for 2 h, and incubated with a primary antibody (Table S4) overnight at 4°C. The next day, the cells were washed with ice-cold PBS 3 times and incubated with a fluorescent secondary antibody (Table S4) at 37°C in the dark for 2 h. After washing with PBS 3 times, the cells were stained with DAPI (Solarbio, Beijing, China) for 10 min, mounted with glycerin, and reviewed and scored under a fluorescence microscope (Olympus).

2.8 | Western blot

Transiently transfected cells were washed with ice-cold PBS and lysed using a lysis buffer (Beyotime) containing a protease-inhibitor cocktail (Beyotime) and a phosphatase-inhibitor cocktail (MedChemExpress). After quantitation using the bicinchoninic acid (BCA) protein assay, equal amounts of protein samples were separated in 10% SDS-PAGE gels and transferred onto polyvinylidene difluoride membranes (Invitrogen). For western blotting, the membranes were blocked with 5% skimmed dry milk solution in TBS-Tween 20 (TBS-T) at room temperature for 2 h and incubated with a primary antibody (Table S4) in 2% BSA in TBS-T at 4°C overnight. The next day, the membranes were washed with TBS-T 3 times and incubated at 37°C with HRP-conjugated anti-mouse/rabbit IgG at a dilution of 1:20 000 (Zsbio) for 2 h. After washing again with TBS-T, the membranes were incubated with Enhanced Chemiluminescence Reagent (Beyotime) to visualize the positive protein bands captured using an enhanced chemiluminescence device (Thermo Fisher Scientific). The results were quantified using ImageLab 3.0 software (Bio-Rad).

2.9 | Cell viability and invasion assays

Changes in the cell viability after gene manipulation were evaluated with an MTT kit (Beyotime). In brief, gene-transfected A549, H1299, H460 and H292 cells were re-plated into 96-well plates in triplicate with 100 μL growth medium and cultured for 0, 24, 48, 72, or 96 h. H1299 cells were re-plated at 2×10^4 cells/well,

A549 cells were re-plated at 3×10^4 cells/well, H460 cells were re-plated at a density of 1.5×10^4 cells/well, while H292 cells were re-plated at a density of 2×10^4 cells/well. At the end of each experiment, 10 μL MTT reagent was added to the cell culture and the cells were cultured for an additional 4 h. The optical absorbance rate was measured using a microplate spectrophotometer (Thermo) at 450 nm and the percentage compared with the control was calculated.

Changes in cell invasion capacity were assessed using 24-well Transwell chambers containing inserts with an 8-μmol/L pore size (Costar) and coated with 100 μL Matrigel (a 1:9 dilution; BD Biosciences). In particular, gene-transfected A549, H1299, H460, and H292 cells were suspended in RPMI-1640 without serum at 8×10^4 cells/mL for A549 cells, 5×10^4 cells/mL for H1299 cells, 2×10^5 cells/mL for H460 cells, and 1×10^5 cells/mL for H292 cells. Next, 100 μL of each cell solution was added to the upper chamber in triplicate, while the lower chamber was filled with 600 μL RPMI-1640 containing 20% FBS. The plates were then incubated in a humidified incubator with 5% CO_2 in air at 37°C for 24 h (48 h for H460 cells). At the end of the incubation period, the cells remaining in the upper chamber were removed with a cotton swab. The cells that migrated to the other side of the chambers were fixed with 4% paraformaldehyde for 10 min and stained with 0.1% crystal violet solution for 10 min. The number of invading cells was counted in 5 randomly selected fields under a light microscope (Leica).

2.10 | Co-immunoprecipitation (Co-IP)-western blot

A549, H1299, H460 and H292 cells with or without gene transfection were collected through an ice-cold PBS wash and lysed in a lysis buffer (see section on western blot). After quantitation, 2 mg of each protein sample were incubated with Protein A+G agarose (Beyotime) at 4°C for 150 min. The samples were washed with TBS-T through centrifugation at 92 *g* in a clinical centrifuge and incubated with anti-*Myc*-tag antibody, anti-LGALS3BP antibody or anti-IgG (as a control; Table S4) at 4°C overnight on a shaking platform. The next day, Protein A+G agarose beads were added to the mixture at 4°C for 6 h to capture the binding antibody complex. After centrifugation, the supernatants were collected and analyzed using western blot.

2.11 | In vivo nude mouse experiment

The animal protocol in this study was approved by the Institutional Animal Care and Use Committee (IACUC) of China Medical University and followed the Guidelines of the Care and Use of Laboratory Animals issued by the Chinese Council on Animal Research. Female BALB/c nude mice at 4 wk of age were purchased from the Charles River company and maintained in a specific pathogen-free (SPF) "barrier" facility and housed under controlled temperature and humidity and alternating 12-h light and dark cycles. The mice received SPF mouse chow and were allowed to drink sterile water ad libitum. For our experiment, the mice were injected subcutaneously in the right forelimb armpit with 1×10^7 stable MZT2A mutant transfected H1299 cells and randomly divided into 4 groups: pNC, pMZT2A, pMZT2A-ΔMOZART2, and pMZT2A-MOZART2 groups. Growth of the subcutaneous tumor xenografts was observed and measured the size of tumors at 7 d, 13 d, 18 d, 22 d, 25 d and 27 d after injection. At the end of the experiment (28 d after injection), tumor xenografts were resected, measured for tumors size, and analyzed for protein expression using western blot.

2.12 | Statistical analysis

Data were summarized as the mean ± standard deviation (SD) and analyzed statistically with the one-way ANOVA to compare the differences among the groups. Mantel-Cox regression analysis was used for survival analysis of immunohistochemical cases. Pearson correlation test was performed to determine the correlation between MZT2A and LGALS3BP levels in NSCLC tissue samples. All statistical analyses were performed using SPSS software (v.22.0; SPSS). A *P*-value ≤ .05 was considered to be statistically significant.

3 | RESULTS

3.1 | Upregulation of MZT2A expression in NSCLCs and association with poor NSCLC prognosis

In this study, we first assessed MZT2A expression in NSCLCs using TCGA data. The initial analysis revealed the differential expression of MZT2A mRNA between NSCLC and normal tissues ($P < .01$) and confirmed the data in the GEPIA database, which showed that MZT2A expression was higher in LUAD and LUSC than in normal tissues ($P < .01$). Our Kaplan-Meier analysis using Kaplan-Meier data revealed that MZT2A expression was associated with poor prognosis for patients with NSCLC (Figure 1A,B).

We next collected our own samples from a cohort of 224 NSCLC patients and analyzed MZT2A expression immunohistochemically. Our data showing that the MZT2A protein was mainly localized in the cytoplasm, although a few cell nuclei were positive for MZT2A protein and MZT2A expression was higher in NSCLC tissues than in normal lung and bronchial tissues which further confirmed TCGA and the GEPIA data (Figure 1C). MZT2A expression was associated with tumor size, lymph node metastasis, and advanced TNM stages (Table 1).

Next, we performed a survival analysis of patients and found that high MZT2A expression was associated with poor prognosis of these patients with lung cancer (Figure 1D).

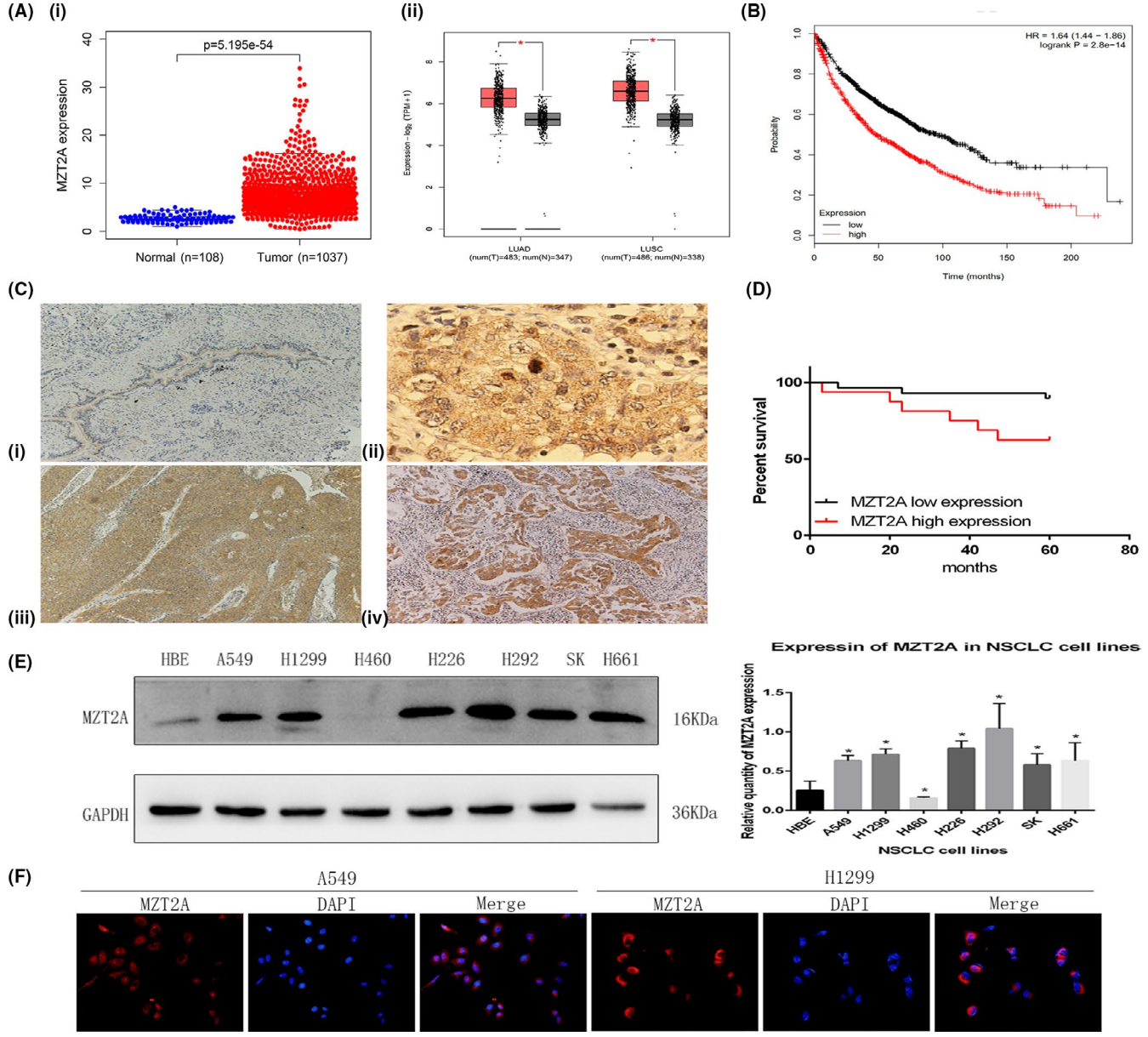

FIGURE 1 MZT2A overexpression and association with poor NSCLC prognosis. A, Differential MZT2A expression in NSCLCs using TCGA data (i) and GEPIA data (ii). LUAD, lung adenocarcinoma; LUSC, lung squamous cell carcinoma. B, Kaplan-Meier survival analysis. High MZT2A expression is associated with poor NSCLC prognosis. C, Immunohistochemistry. MZT2A expression in our cohort of 132 NSCLC cases was analyzed. i, Weak MZT2A expression in normal bronchial epithelium. ii, Strong staining of MZT2A in mitosis-stage cells. iii, iv, MZT2A expression in LUSC and adenocarcinoma cells. D, Western blot. NSCLC cell lines and HBE cells were grown and harvested for western blot analysis. The data showed that MZT2A expression was highest in H292 cells and lowest expressed in H460 cells. The graph is the quantified data for the western blots. E, Immunofluorescence. NSCLC A549 and H1299 cells were grown and immunostained with an MZT2A antibody. The data show that MZT2A was mainly localized in the cytoplasm with some staining in the nuclei

3.2 | MZT2A promotion of NSCLC cell malignant behaviors in vitro

We assessed the levels of MZT2A protein in different lung cancer cell lines and found that the expression of MZT2A protein was higher in cancer cell lines than in normal cells, with the exception of NCI-H460 cells (Figure 1E). For our subsequent experiments, we selected the A549, H1299, H460 and H292 cell lines with different levels of MZT2A expression; results showed that MZT2A expression was the highest and lowest in H292 and H460 cell lines, respectively. Our immunocytochemical staining further confirmed the cytoplasmic localization of MZT2A in the centrosomes and cytoplasm, although some nuclei were also positive for MZT2A in NSCLC cells (Figures 1F and S1A).

We further explored the effect of MZT2A overexpression and knockdown on the regulation of NSCLC cell viability, invasion, and gene expression. We first confirmed MZT2A overexpression and knockdown with MZT2A cDNA and siRNA transfection in NSCLC cells, detected using western blot and RT-qPCR (Figures 2A,B and

TABLE 1 Association of MZT2A expression with clinicopathological data from patients

Variables	N	MZT2A expression high	MZT2A expression low	*P*-value
Age (y)				
≤60	121	50	71	.2151
>60	103	34	69	
Gender				
Male	154	75	79	.4711
Female	70	30	40	
Histological type				
Squamous cell carcinoma	108	65	43	.1083
Adenocarcinoma	116	57	59	
Tumor differentiation				
Well	134	55	79	.2177
Poor	90	45	45	
Tumor size (cm)				
≤2	113	47	66	.0034
>2.5	111	68	43	
Lymph node metastasis				
Negative	134	46	88	.0002
Positive	90	54	36	
TNM stage				
I	114	78	36	<.01
II-III	110	46	64	

S1B). Next, we performed a cell viability MTT assay and found that the cell viability was reduced after knockdown of MZT2A expression in A549, H1299, and H292 cell lines, whereas tumor cell viability was upregulated following MTZ2A overexpression in A549, H1299 and H460 cell lines ($P < .05$; Figures 2C and S1C). Furthermore, tumor cell invasion capacity was suppressed after knockdown of MTZ2A expression, whereas MTZ2A overexpression enhanced tumor cell invasion capacity compared with that of control cells ($P < .05$; Figures 2D and S1D). In addition, the protein and mRNA levels of cyclinD1, CDK4, CDK6, RhoA, and vimentin expression were downregulated by MZT2A siRNA, whereas MZT2A cDNA had the opposite effect on the expression of these proteins compared with levels in the control cells ($P < .05$; Figures 2E,F and S1B).

3.3 | MZT2A regulation of NSCLC cell malignant behaviors via Akt phosphorylation

After screening various signal transduction molecules, we speculated that Akt signaling might modulate the MZT2A-induced malignant behaviors of A549, H1299, and H460 cells. We found that the level of phosphorylated-Akt protein was reduced after MTZ2A siRNA transfection, whereas MTZ2A cDNA had the opposite effect on Akt phosphorylation ($P < .05$; Figures 3A and S1B). However, total Akt protein and mRNA levels showed no significant changes in cells transfected with MTZ2A siRNA or cDNA ($P > .05$; Figures 3A,B and S1B).

We added treatment with an inhibitor (LY294002) to block Akt signaling in our experimental setting and found that LY294002 treatment suppressed Akt phosphorylation but did not alter total Akt level (Figures 3C and S1E). We also found that the degree of increase in the phosphorylated-Akt level after MZT2A cDNA transfection was reduced by LY294002 treatment, but that total Akt protein level barely changed ($P < .05$; Figures 3C and S1E). The promoting effect of MZT2A overexpression on NSCLC cell viability and invasion was also inhibited by LY294002 ($P < .05$; Figures 3D, E and S1F,G).

3.4 | MZT2A activation of Akt signaling via galectin-3-binding protein (LGALS3BP)

To further explore the underlying molecular events, we searched various biomedical databases and retrieved data suggesting that LGALS3BP was linked to MZT2A activation of the Akt protein. We then performed Co-IP-western blot analysis and confirmed the interaction between MZT2A and LGALS3BP in NSCLC cells (Figures 4A and S1H). Immunohistochemistry results of LGALS3BP showed that LGALS3BP protein was mainly localized in the cytoplasm, and were consistent with localization of MZT2A in cells. Our Pearson correlation analysis of immunohistochemical data on MTZ2A and LGALS3BP also confirmed this relationship ($P < .05$; Figure 4B). Co-transfection of MZT2A cDNA and LGALS3BP siRNA into NSCLC cells showed that, compared with

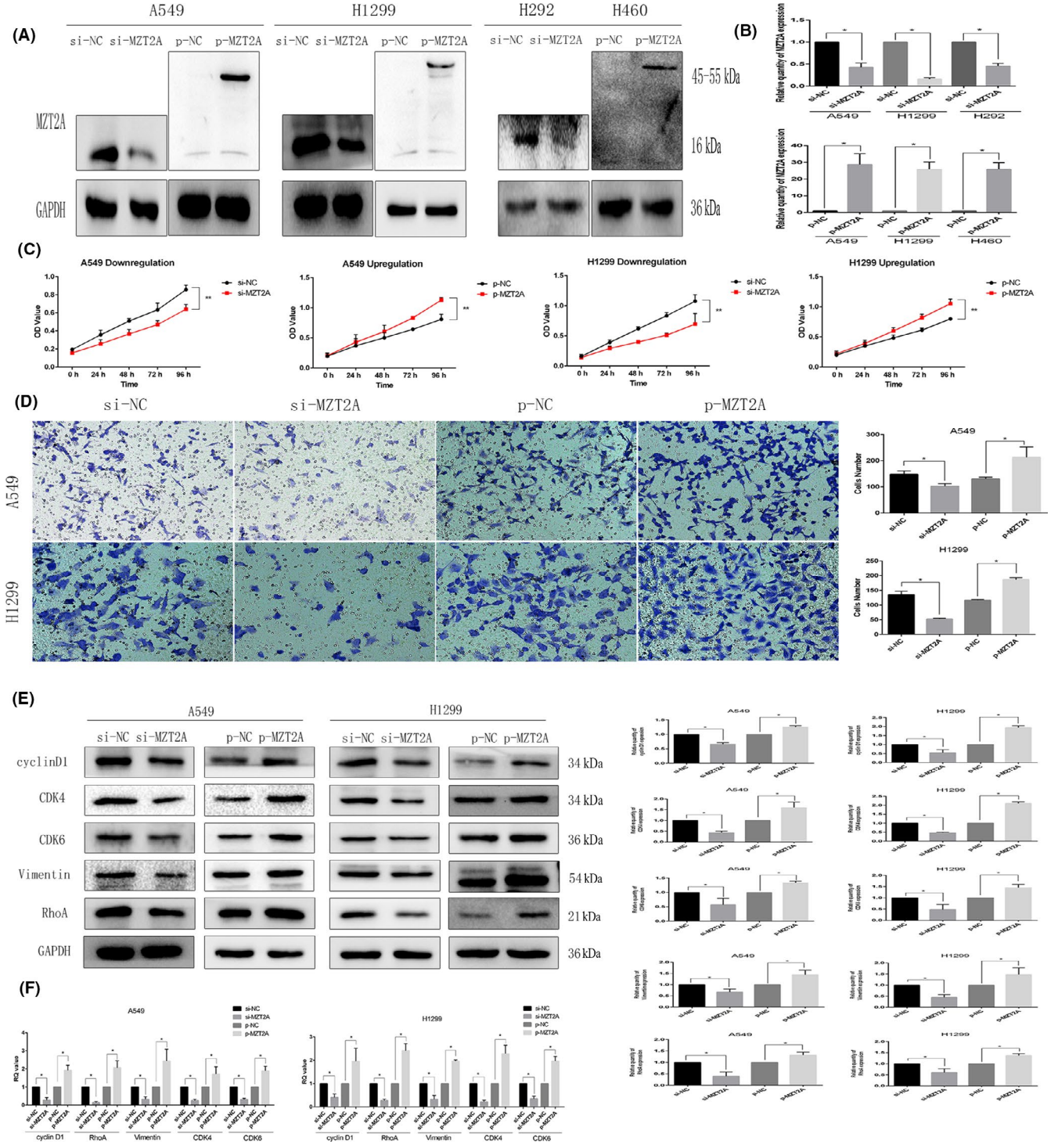

FIGURE 2 MZT2A promotion of NSCLC cell viability and invasion, as well as regulation of protein expression in A549 and H1299 cells. A, Western blot. NSCLC A549 and H1299 cells were grown, transfected with MZT2A cDNA or siRNA, and subjected to western blot analysis. The data showed that MZT2A cDNA or siRNA transfection, respectively, upregulated and downregulated MZT2A expression. Graphs show the quantified data. B, RT-qPCR. NSCLC A549 and H1299 cells were grown, transfected with MZT2A cDNA or siRNA, and subjected to RT-qPCR. C, Cell viability MTT assay. NSCLC A549 and H1299 cells were grown, transfected with MZT2A cDNA or siRNA, and subjected to cell viability assays. Data show that the upregulation or downregulation of MZT2A expression promoted or reduced NSCLC cell viability. D, Transwell invasion assay. NSCLC A549 and H1299 cells were grown, transfected with MZT2A cDNA or siRNA, and subjected to Transwell assays. Graphs show the quantified data. E, Western blot. NSCLC A549 and H1299 cells were grown, transfected with MZT2A cDNA or siRNA, and subjected to western blot analysis of the proteins associated with cell proliferation and invasion. Graphs show the quantified data. F, RT-qPCR. NSCLC A549 and H1299 cells were grown, transfected with MZT2A cDNA or siRNA, and subjected to RT-qPCR analysis of the gene associated with cell proliferation and invasion. Graphs show the quantified data

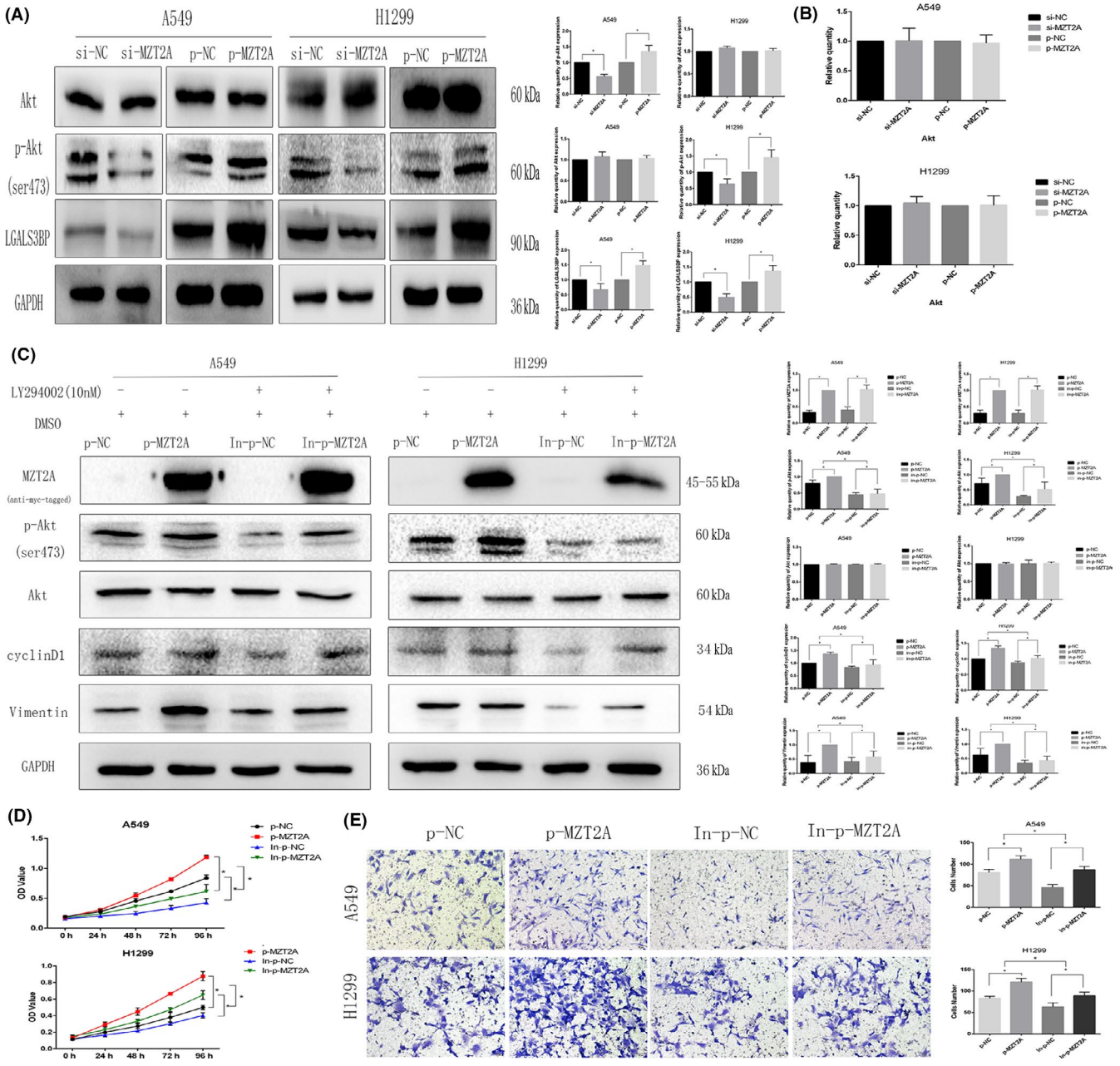

FIGURE 3 MZT2A regulation of Akt phosphorylation in NSCLC. A, Western blot. NSCLC A549 and H1299 cells were grown, transfected with MZT2A cDNA or siRNA, and subjected to western blot analysis. Graphs show the quantified data. B, RT-qPCR. NSCLC A549 and H1299 cells were grown, transfected with MZT2A cDNA or siRNA, and subjected to RT-qPCR. C, Western blot. A549 and H1299 cells were grown, transfected with MZT2A cDNA, treated with or without the selective Akt inhibitor LY294002, and subjected to western blot analysis. Graphs show the quantified data. D, Cell viability MTT assay: A549 and H1299 cells were grown, transfected with MZT2A cDNA, treated with or without the selective Akt inhibitor LY294002, and subjected to MTT assays. E, Transwell assay. A549 and H1299 cells were grown, transfected with MZT2A cDNA, treated with or without the selective Akt inhibitor LY294002, and subjected to Transwell assays. Graphs show the quantified data

MZT2A cDNA alone, LGALAS3BP siRNA inhibited the promoting effect of MZT2A on the level of Akt phosphorylation, whereas LGALS3BP siRNA alone did not alter the level of MZT2A protein ($P < .05$; Figures 4C and S1I). The level of LGALS3BP protein was upregulated after MZT2A cDNA transfection in NSCLC cells ($P < .05$; Figures 4C and S1I). In addition, the promoting effects of MZT2A on NSCLC cell viability and invasion were also reduced by LGALS3BP siRNA ($P < .05$; Figures 4D,E and S1J,K).

3.5 | MZT2A activation of LGALS3BP and Akt phosphorylation via the MOZART2 domain

To further investigate the molecular mechanisms underlying the effects of MZT2A and LGALS3BP in NSCLC cells, we constructed 2 MZT2A mutant vectors and performed Co-IP-western blot assays (Figure 5A,B). Our data showed positive results in groups transfected with MZT2A-WT and MZT2A-MOZART2 vectors (Figures 5C,D and

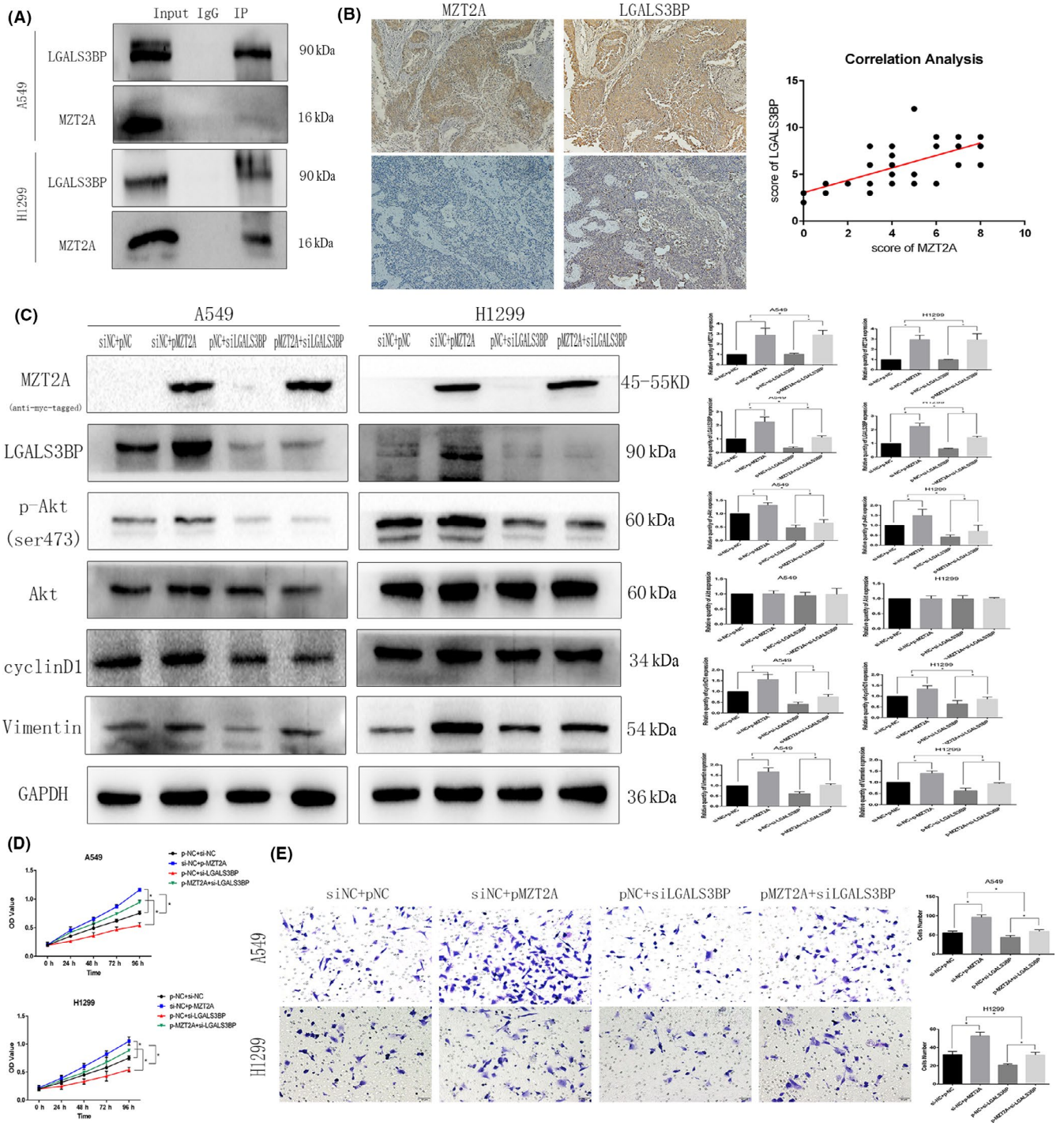

FIGURE 4 MZT2A-activated Akt signal transduction via LGALS3BP. A, Co-IP-western blot. A549 and H1299 cells were grown and subjected to Co-IP-western blot analysis to detect the intact interaction between MZT2A and LGALS3BP proteins B, Immunohistochemistry and Pearson correlation analysis. NSCLC tissue sections were immunostained with an anti-MZT2A or LGALS3BP antibody and the expression of MZT2A and LGALS3BP protein was scored as high or low. Tissue sections were subjected to Pearson correlation analysis (shown in the graph; $P < .05$). C, Western blot. A549 and H1299 cells were grown, transfected with MZT2A cDNA and/or LGALS3BP siRNA, and subjected to western blot analysis. D, Cell viability MTT assay. A549 and H1299 cells were grown, transfected with MZT2A cDNA and/or LGALS3BP siRNA, and subjected to MTT assays. E, Transwell assay. A549 and H1299 cells were grown, transfected with MZT2A cDNA and/or LGALS3BP siRNA, and subjected to Transwell assays. Graph shows the quantified data

S2A). Specifically, without the MOZART2 domain, MZT2A could not bind to or regulate LGALS3BP expression in tumor cells. Our western blot data showed that, only with an intact MOZART2 domain, MTZ2A was able to induce LGALS3BP expression and Akt phosphorylation ($P < .05$; Figures 5E and S2B) as well as promote tumor cell viability and invasion ($P < .05$; Figures 5F,G and S2C,D).

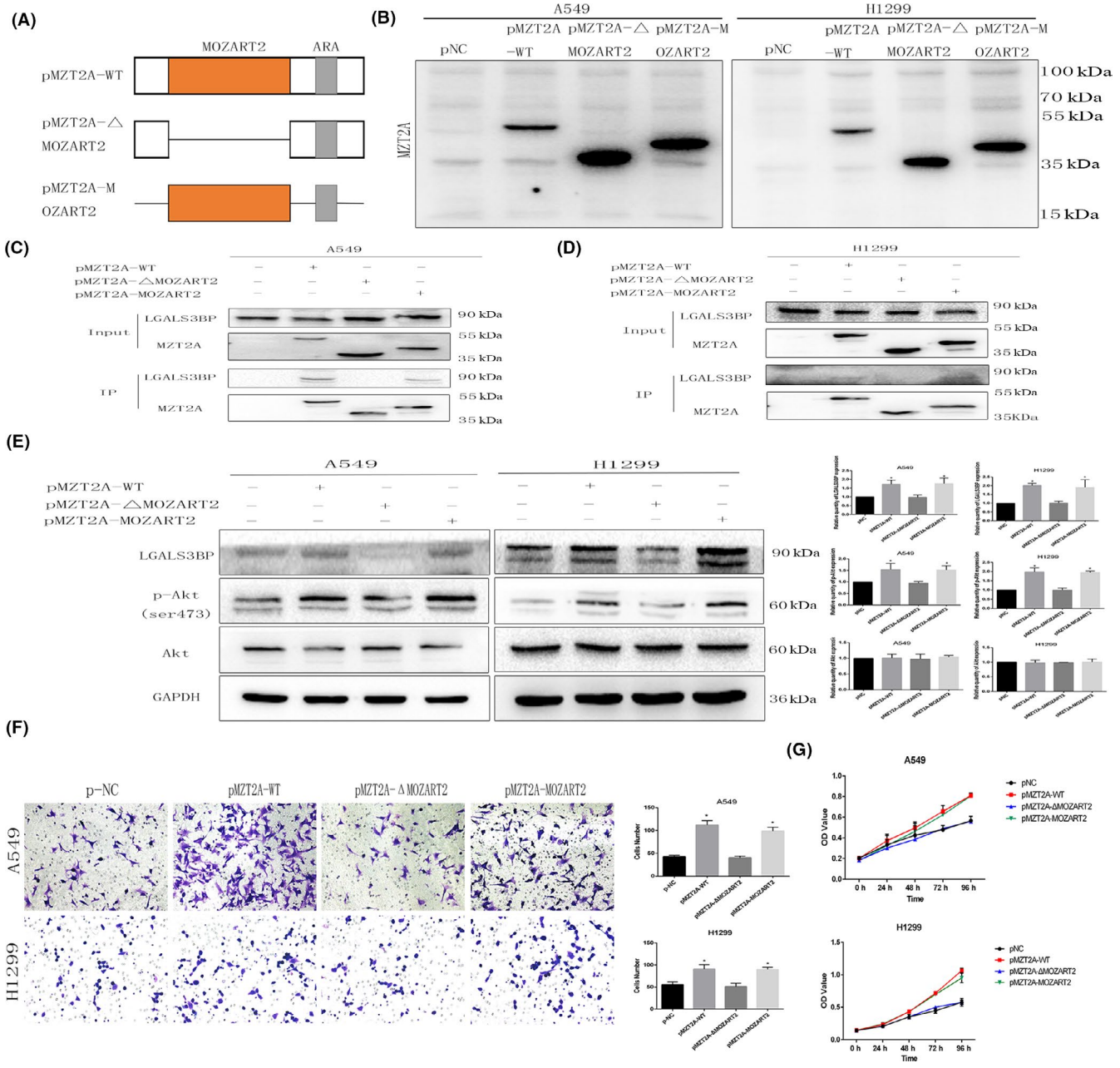

FIGURE 5 The MZT2A functional domain MOZART2 mediates MZT2A functions in the regulation of Akt phosphorylation. A, Illustration of our creation of 2 mutated MZT2A MOZART2 domain constructs. ARS: antibody recognition sequences B, Western blot. A549 and H1299 cells were grown and transfected with the 2 mutated MZT2A cDNA constructs, and then were subjected to western blot analysis. C, D, Co-IP-western blot. A549 and H1299 cells were grown, transfected with the 2 mutated MZT2A cDNA, and subjected to Co-IP-western blot. E, Western blot. A549 and H1299 cells were grown, transfected with the 2 mutated MZT2A cDNAs, and subjected to Co-IP-western blot analysis. F, Transwell assay. A549 and H1299 cells were grown, transfected with the 2 mutated MZT2A cDNAs, and subjected to Transwell assays. Graphs show the quantified data. G, Cell viability MTT assay. A549 and H1299 cells were grown, transfected with the 2 mutated MZT2A cDNAs, and subjected to MTT assays

3.6 | MZT2A activation of Akt phosphorylation in vivo

H1299 cells after stable transfection with negative control and mutant *MZT2A* vectors were injected into nude mice. After 28 d, we observed that tumor sizes with the MZT2A-WT and MZT2A-MOZART2 vectors group were larger than that of the negative control and MZT2A-ΔMOZART2 groups ($P < .05$; Figure 6A). We measured the changes in tumor sizes at 7, 13, 18, 22, 25, and 27 d after injection; the growth curve also confirmed that MZT2A could exert its biological function of promoting tumor growth only when the MOZART2 domain was present ($P < .05$; Figure 6B). Western blot data showed

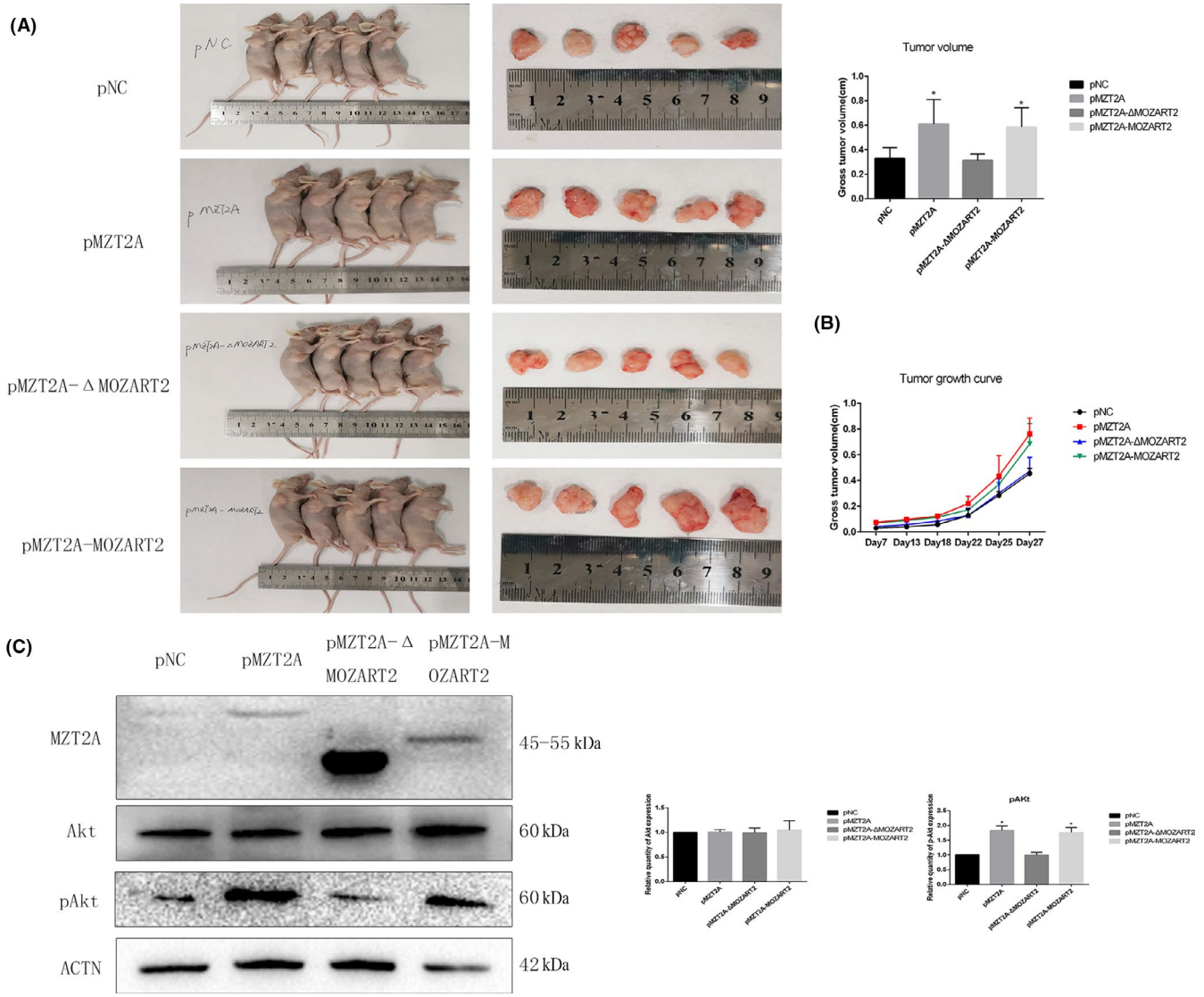

FIGURE 6 MZT2A activation of Akt phosphorylation in vivo. A, Nude mice bearing tumors (shown in the graph; $P < .05$). B, Tumor growth curve. Tumor size were measured at 7, 13, 18, 22, 25, and 27 d after injection. C, Western blot. Tumor proteins subjected to western blot analysis

that expression of p-Akt proteins was significantly increased in the MZT2A-WT and MZT2A-MOZART2 groups ($P < .05$; Figure 6C). This result was consistent with the results of our in vitro data.

4 | DISCUSSION

In the current study, we identified differential MZT2A expression in NSCLC tissues vs. normal lung tissues and the association between MZT2A expression and NSCLC prognosis. We then overexpressed or knocked down MZT2A expression in NSCLC cells using MZT2A cDNA and siRNA, respectively, to assess the oncogenic activity of MTZ2A in NSCLCs. We found that both MZT2A mRNA and protein were upregulated in NSCLC tissues, which was associated with larger NSCLC size, lymph node metastasis, advanced TNM stages of NSCLCs, and poor NSCLC prognosis. In vitro, MZT2A protein was highly expressed in all NSCLC cell lines except one (NCI-H460) compared with expression in normal bronchial cells. MZT2A overexpression promoted NSCLC cell viability and invasion, whereas MTZ2A siRNA transfection had the opposite effect. Moreover, MZT2A induced Akt phosphorylation to promote NSCLC proliferation and invasion, and these effects were blocked by the selective Akt inhibitor LY294002. MTZ2A also upregulated LGALS3BP expression through the MOZART2 domain, whereas LGALS3BP siRNA suppressed MTZ2A-induced Akt phosphorylation in NSCLC cells. Our nude mouse experiment data showed consistency with our in vitro data. In conclusion, MZT2A was overexpressed in NSCLC tissues, which was associated with poor NSCLC prognosis. MZT2A overexpression promoted NSCLC cell viability and invasion through LGALS3BP upregulation and Akt phosphorylation, indicating that MZT2A possesses

oncogenic activities in NSCLCs in vitro and in vivo. Future studies should further evaluate MTZ2A as a biomarker for the prediction of NSCLC prognosis or as a target for the control of NSCLCs.

Previous studies have shown that MZT2A can induce the proliferation of various types of human cancer cells.[22,24] It has been demonstrated that microtubules can regulate tumor cell metastasis and invasion.[26] As a component of microtubules, we propose that MZT2A not only functions to regulate the cell cycle and cell proliferation as reported in the literature,[24,27] but also affects the mobility of NSCLC cells (our current data). The changes caused by MZT2A in the malignant behaviors of NSCLC cell illustrated in our current study were due to the induction of Akt phosphorylation. Indeed, high levels of Akt phosphorylation have been detected in various human cancers and play a role in many different biological activities during the transformation of normal cells to cancerous cells.[28-30] For example, Akt can promote cell cycle progression,[31] and cell proliferation [32] as well as cell survival.[33] Akt regulates lysosomal biogenesis, autophagy, and angiogenesis, all of which are important in human carcinogenesis.[34,35] Akt activation is also associated with many malignancies.[36,37] Previous studies have shown that Akt phosphorylation is increased in many tumors, including NSCLCs.[38,39] Our current study further confirmed the role of Akt in the promotion of NSCLC cell proliferation and invasion. We demonstrated that MZT2A could promote Akt phosphorylation; however, MZT2A is a protein in the centrosome with no kinase activity, suggesting that the MZT2A activation of Akt is indirect. Therefore, we speculated that there might be another molecule that serves as a bridge (link) between MZT2A and Akt to induce Akt phosphorylation. We searched protein–protein interaction databases and identified LGALS3BP as a potential linker. Indeed, our Co-IP-western blot and immunohistochemical data supported this speculation by showing a physical interaction between MZT2A and LGALS3BP protein. Thereafter, we found that LGALS3BP was able to upregulate Akt signaling activity by increasing Akt phosphorylation. A literature search uncovered 2 theories about the specific mechanism used by LGALS3BP for the regulation of Akt phosphorylation. One theory is that LGALS3BP induces Akt phosphorylation at the Ser473 site through integrins.[40] The other theory is that LGALS3BP binds to galectin 3 to activate phosphoinositide-dependent kinase 1 and in turn upregulates the level of Akt phosphorylation at the Thr308 site.[41,42] In our current study, we detected MZT2A activation of Akt phosphorylation at the Thr308 site. However, our results indicated that the Thr308 site phosphorylation induced by MZT2A was not stable, whereas the change caused by MZT2A at the Ser473 phosphorylation site appeared to be steady. Indeed, MZT2A is a protein with a small molecular weight and previous studies have focused on the role of MZT2A in cell mitosis, especially the formation of the spindle.[22,24,27] In this regard, functional descriptions of the unique MZT2A MOZART2 domain were also focused on this process. Although MZT2A depletion has not been reported to affect the γ-TuRC assembly, it interferes with γ-TuRC recruitment and microtubule nucleation in the interphase centrosomes, but does not disrupt the general centrosome structure, indicating that MZT2A plays a role in the organization of the interphase microtubule network.[22] In our current study, we mutated the MOZART2 domain and observed that the mutation disrupted Akt phosphorylation as well as NSCLC cell viability and invasion capacity, indicating that the MOZART2 domain is necessary for MZT2A to function in NSCLC cells in vitro and in vivo.

However, our current study is merely a proof of principle and several limitations exist, for example most of our data are descriptive and the study lacks precise mechanism experiments. NSCLC development is a multi-factorial process. The upregulation of MZT2A expression may also modulate the expression and activity of other proteins in NSCLC cells to promote NSCLC development and progression. However, our current data only showed one example of MZT2A action in NSCLC cells. In future studies, we will explore the cause of MZT2A overexpression in NSCLCs and the underlying molecular mechanisms of MZT2A-induced NSCLC development and progression.

In conclusion, our current data, for the first time, demonstrated that overexpression of MZT2A mRNA and protein was associated with NSCLC progression and poor prognosis. In vitro and in vivo, MZT2A promoted NSCLC malignant behaviors by increasing Akt phosphorylation via LGALS3BP in NSCLC cells. We also identified the importance of the MOZART2 domain for a functional MZT2A protein in NSCLC.

ACKNOWLEDGMENTS

The authors would like to thank Medjaden Bioscience Limited Company (Hong Kong, China) for help in editing and proofreading our manuscript.

CONFLICT OF INTEREST

The authors declare that there is no conflict of interest in this work.

AUTHOR CONTRIBUTIONS

Huanxi Wang, Hongjiu Ren, and Xueshan Qiu conceived and designed the experiments; Huanxi Wang, Zifang Zou, and Yu Cheng prepared the manuscript; Huanxi Wang, Xizi Jiang, Yujiao Hu, Zongang Liu, Jiameng Zhang and Qiongzi Wang performed the experiments; Yao Zhang and Hongbo Su analyzed the data.

ETHICAL APPROVAL

This study was approved by the Medical Research Ethics Committee of China Medical University and informed consent was obtained from all patients.

DATA AVAILABILITY STATEMENT

All data generated or analyzed during this study are included in this article. Further details are available from the corresponding author upon request.

ORCID

Xizi Jiang https://orcid.org/0000-0002-8676-4153
Xueshan Qiu https://orcid.org/0000-0001-9481-8249

REFERENCES

1. Bray F, Ferlay J, Soerjomataram I, Siegel RL, Torre LA, Jemal A. Global cancer statistics 2018: GLOBOCAN estimates of incidence

and mortality worldwide for 36 cancers in 185 countries. *CA Cancer J Clin*. 2018;68(6):394-424.
2. Siegel RL, Miller KD, Jemal A. Cancer statistics, 2019. *CA Cancer J Clin*. 2019;69(1):7-34.
3. Torre LA, Bray F, Siegel RL, Ferlay J, Lortet-Tieulent J, Jemal A. Global cancer statistics, 2012. *CA Cancer J Clin*. 2015;65(2):87-108.
4. Torre LA, Siegel RL, Jemal A. Lung cancer statistics. *Adv Exp Med Biol*. 2016;893:1-19.
5. Goldstraw P, Ball D, Jett JR, et al. Non-small-cell lung cancer. *Lancet*. 2011;378(9804):1727-1740.
6. Travis WD. Pathology of lung cancer. *Clin Chest Med*. 2011;32(4):669-692.
7. Hoseok I, Cho JY. Lung cancer biomarkers. *Adv Clin Chem*. 2015;72:107-170.
8. Pellegrini F, Budman DR. Review: tubulin function, action of antitubulin drugs, and new drug development. *Cancer Invest*. 2005;23(3):264-273.
9. Correia JJ, Wilson L. Microtubules and microtubule-associated proteins. Preface. *Methods Cell Biol*. 2013;115.xix–xx.
10. Goodson HV, Jonasson EM. Microtubules and microtubule-associated proteins. *Cold Spring Harb Perspect Biol*. 2018;10(6):a022608.
11. Tovey CA, Conduit PT. Microtubule nucleation by gamma-tubulin complexes and beyond. *Essays Biochem*. 2018;62(6):765-780.
12. Rodrigues-Ferreira S, Molina A, Nahmias C. Microtubule-associated tumor suppressors as prognostic biomarkers in breast cancer. *Breast Cancer Res Treat*. 2020;179(2):267-273.
13. Nayak L, DeAngelis LM, Robins HI, et al. Multicenter phase 2 study of patupilone for recurrent or progressive brain metastases from non-small cell lung cancer. *Cancer*. 2015;121(23):4165-4172.
14. Ferrara R, Pilotto S, Peretti U, et al. Tubulin inhibitors in non-small cell lung cancer: looking back and forward. *Expert Opin Pharmacother*. 2016;17(8):1113-1129.
15. Tagliamento M, Genova C, Rossi G, et al. Microtubule-targeting agents in the treatment of non-small cell lung cancer: insights on new combination strategies and investigational compounds. *Expert Opin Investig Drugs*. 2019;28(6):513-523.
16. Cheng CC, Clark Lai YC, Lai YS, et al. Cell pleomorphism and cytoskeleton disorganization in human liver cancer. *In Vivo*. 2016;30(5):549-555.
17. Huang M, Ma X, Shi H, et al. FAM83D, a microtubule-associated protein, promotes tumor growth and progression of human gastric cancer. *Oncotarget*. 2017;8(43):74479-74493.
18. Overby A, Zhao CM, Bones AM, Chen D. Naturally occurring phenethyl isothiocyanate-induced inhibition of gastric cancer cell growth by disruption of microtubules. *J Gastroenterol Hepatol*. 2014;29(Suppl 4):99-106.
19. Cetti E, Di Marco T, Mauro G, et al. Mitosis perturbation by MASTL depletion impairs the viability of thyroid tumor cells. *Cancer Lett*. 2019;442:362-372.
20. Jordan MA, Wilson L. Microtubules as a target for anticancer drugs. *Nat Rev Cancer*. 2004;4(4):253-265.
21. Yang H, Ganguly A, Cabral F. Inhibition of cell migration and cell division correlates with distinct effects of microtubule inhibiting drugs. *J Biol Chem*. 2010;285(42):32242-32250.
22. Hutchins JRA, Toyoda Y, Hegemann B, et al. Systematic analysis of human protein complexes identifies chromosome segregation proteins. *Science*. 2010;328(5978):593-599.
23. Jiang P, Zheng S, Lu L. Mitotic-spindle organizing protein MztA mediates septation signaling by suppressing the regulatory subunit of protein phosphatase 2A-ParA in *Aspergillus nidulans*. *Front Microbiol*. 2018;9:988.
24. Teixido-Travesa N, Villen J, Lacasa C, et al. The gammaTuRC revisited: a comparative analysis of interphase and mitotic human gammaTuRC redefines the set of core components and identifies the novel subunit GCP8. *Mol Biol Cell*. 2010;21(22):3963-3972.
25. Goldstraw P, Chansky K, Crowley J, et al. The IASLC lung cancer staging project: proposals for revision of the TNM stage groupings in the forthcoming (Eighth) edition of the TNM classification for lung cancer. *J Thorac Oncol*. 2016;11(1):39-51.
26. Garcin C, Straube A. Microtubules in cell migration. *Essays Biochem*. 2019;63(5):509-520.
27. Liu P, Choi YK, Qi RZ. NME7 is a functional component of the gamma-tubulin ring complex. *Mol Biol Cell*. 2014;25(13):2017-2025.
28. Ersahin T, Tuncbag N, Cetin-Atalay R. The PI3K/AKT/mTOR interactive pathway. *Mol Biosyst*. 2015;11(7):1946-1954.
29. Liu L, Wang Y, Yu Q. The PI3K/Akt signaling pathway exerts effects on the implantation of mouse embryos by regulating the expression of RhoA. *Int J Mol Med*. 2014;33(5):1089-1096.
30. Porta C, Paglino C, Mosca A. Targeting PI3K/Akt/mTOR signaling in cancer. *Front Oncol*. 2014;4:64.
31. Chen J, Somanath PR, Razorenova O, et al. Akt1 regulates pathological angiogenesis, vascular maturation and permeability in vivo. *Nat Med*. 2005;11(11):1188-1196.
32. Kandel ES, Skeen J, Majewski N, et al. Activation of Akt/protein kinase B overcomes a G(2)/m cell cycle checkpoint induced by DNA damage. *Mol Cell Biol*. 2002;22(22):7831-7841.
33. Song G, Ouyang G, Bao S. The activation of Akt/PKB signaling pathway and cell survival. *J Cell Mol Med*. 2005;9(1):59-71.
34. Sardiello M, Palmieri M, di Ronza A, et al. A gene network regulating lysosomal biogenesis and function. *Science*. 2009;325(5939):473-477.
35. Somanath PR, Razorenova OV, Chen J, Byzova TV. Akt1 in endothelial cell and angiogenesis. *Cell Cycle*. 2006;5(5):512-518.
36. Auguste A, Bessiere L, Todeschini A, et al. Molecular analyses of juvenile granulosa cell tumors bearing AKT1 mutations provide insights into tumor biology and therapeutic leads. *Hum Mol Genet*. 2015;24(23):6687-6698.
37. Sykes SM, Lane SW, Bullinger L, et al. AKT/FOXO signaling enforces reversible differentiation blockade in myeloid leukemias. *Cell*. 2011;146(5):697-708.
38. Liao SY, Kuo IY, Chen YT, et al. AKT-mediated phosphorylation enhances protein stability and transcription activity of ZNF322A to promote lung cancer progression. *Oncogene*. 2019;38(41):6723-6736.
39. Revathidevi S, Munirajan AK. Akt in cancer: mediator and more. *Semin Cancer Biol*. 2019;59:80-91.
40. Stampolidis P, Ullrich A, Iacobelli S. LGALS3BP, lectin galactoside-binding soluble 3 binding protein, promotes oncogenic cellular events impeded by antibody intervention. *Oncogene*. 2015;34(1):39-52.
41. Zhang X, Ding H, Lu Z, et al. Increased LGALS3BP promotes proliferation and migration of oral squamous cell carcinoma via PI3K/AKT pathway. *Cell Signal*. 2019;63:109359.
42. Oka N, Nakahara S, Takenaka Y, et al. Galectin-3 inhibits tumor necrosis factor-related apoptosis-inducing ligand-induced apoptosis by activating Akt in human bladder carcinoma cells. *Can Res*. 2005;65(17):7546-7553.

SUPPORTING INFORMATION

Additional supporting information may be found online in the Supporting Information section.

How to cite this article: Wang H, Jiang X, Cheng Y, et al. MZT2A promotes NSCLC viability and invasion by increasing Akt phosphorylation via the MOZART2 domain. *Cancer Sci*. 2021;112:2210–2222. https://doi.org/10.1111/cas.14900